

*ARMY RESEARCH LABORATORY*



**Unsteady Numerical Simulations of Subsonic Flow  
Over a Projectile With Jet Interaction**

**Jubaraj Sahu**

**ARL-TR-2975**

**MAY 2003**

## **NOTICES**

### **Disclaimers**

The findings in this report are not to be construed as an official Department of the Army position unless so designated by other authorized documents.

Citation of manufacturers' or trade names does not constitute an official endorsement or approval of the use thereof.

**DESTRUCTION NOTICE** Destroy this report when it is no longer needed. Do not return it to the originator.

# **Army Research Laboratory**

Aberdeen Proving Ground, MD 21005-5066

---

---

ARL-TR-2975

May 2003

---

## **Unsteady Numerical Simulations of Subsonic Flow Over a Projectile With Jet Interaction**

**Jubaraj Sahu**  
**Weapons & Materials Research Directorate**

---

Approved for public release; distribution is unlimited.

---

---

INTENTIONALLY LEFT BLANK

# REPORT DOCUMENTATION PAGE

*Form Approved*  
*OMB No. 0704-0188*

Public reporting burden for this collection of information is estimated to average 1 hour per response, including the time for reviewing instructions, searching existing data sources, gathering and maintaining the data needed, and completing and reviewing the collection of information. Send comments regarding this burden estimate or any other aspect of this collection of information, including suggestions for reducing the burden, to Department of Defense, Washington Headquarters Services, Directorate for Information Operations and Reports (0704-0188), 1215 Jefferson Davis Highway, Suite 204, Arlington, VA 22202-4302. Respondents should be aware that notwithstanding any other provision of law, no person shall be subject to any penalty for failing to comply with a collection of information if it does not display a currently valid OMB control number.

**PLEASE DO NOT RETURN YOUR FORM TO THE ABOVE ADDRESS.**

1. REPORT DATE (DD-MM-YYYY) May 2003		2. REPORT DATE Final		3. DATES COVERED (From - To)	
4. TITLE AND SUBTITLE  Unsteady Numerical Simulations of Subsonic Flow Over a Projectile With Jet Interaction				5a. CONTRACT NUMBER	
				5b. GRANT NUMBER	
				5c. PROGRAM ELEMENT NUMBER	
6. AUTHOR(S)  Sahu, J. (ARL)				5d. PROJECT NUMBER 1L1612618AH80	
				5e. TASK NUMBER	
				5f. WORK UNIT NUMBER	
7. PERFORMING ORGANIZATION NAME(S) AND ADDRESS(ES) U.S. Army Research Laboratory Weapons & Materials Research Directorate Aberdeen Proving Ground, MD 21005-5066				8. PERFORMING ORGANIZATION REPORT NUMBER  ARL-TR-2975	
9. SPONSORING/MONITORING AGENCY NAME(S) AND ADDRESS(ES)				10. SPONSOR/MONITOR'S ACRONYM(S)	
				11. SPONSOR/MONITOR'S REPORT NUMBER(S)	
12. DISTRIBUTION/AVAILABILITY STATEMENT  Approved for public release; distribution is unlimited.					
13. SUPPLEMENTARY NOTES					
14. ABSTRACT  This report describes a computational study undertaken to consider the aerodynamic effect of synthetic jets as a means to provide the control authority needed to maneuver a projectile at low subsonic speeds. The time-accurate Navier-Stokes computational technique has been used to obtain numerical solutions for the unsteady jet interaction flow field for a projectile at a subsonic speed, Mach = 0.11, and several angles of attack from 0° to 4°. Qualitative flow field features show the interaction of the time-dependent jet with the free stream flow. Numerical results show the effect of the jet on the flow field, surface pressures and aerodynamic coefficients. Unsteady numerical results have been obtained for a two-dimensional jet flow and compared with experimental data for validation. The same unsteady jet modeling technique has been applied to a subsonic projectile. These numerical results are being assessed to determine if synthetic jets can be used to provide the control authority needed for maneuvering munitions to hit the targets with precision.					
5. SUBJECT TERMS chimera    computational fluid dynamics    projectile and missile aerodynamics    structured grids    unstructured grids					
6. SECURITY CLASSIFICATION OF			17. LIMITATION OF ABSTRACT  UL	18. NUMBER OF PAGES  25	19a. NAME OF RESPONSIBLE PERSON Jubaraj Sahu
i. REPORT Unclassified	b. ABSTRACT Unclassified	c. THIS PAGE Unclassified			19b. TELEPHONE NUMBER (Include area code) 410-278-3707

INTENTIONALLY LEFT BLANK

---

## Contents

---

<b>List of Figures</b>	v
<b>Acknowledgments</b>	vii
<b>1. Introduction</b>	1
<b>2. Solution Technique</b>	2
2.1 Dual Time Stepping . . . . .	4
2.2 Unsteady Jet Boundary Condition . . . . .	4
2.3 Hybrid RANS-LES Model . . . . .	5
<b>3. Results</b>	6
<b>4. Concluding Remarks</b>	15
<b>5. References</b>	16

---

## List of Figures

---

Figure 1. Schematic of a 2-D unsteady jet in the experiment . . . . .	7
Figure 2. Contours of velocity components (u, v) and vorticity (from left to right) . . . . .	7
Figure 3. Variation of time-averaged centerline jet velocity with distance from the wall . . . . .	7
Figure 4. Projectile model geometry . . . . .	8
Figure 5. Aft-end geometry showing the jet location . . . . .	8
Figure 6. Computational grid near the projectile . . . . .	9
Figure 7. Computed pressures, jet off, $M = 0.11$ , $\alpha = 0^\circ$ . . . . .	10
Figure 8. Computed velocity vectors, jet off, $M = 0.11$ , $\alpha = 0^\circ$ . . . . .	10
Figure 9. Instantaneous computed velocity vectors, jet on, $M = 0.11$ , $\alpha = 0^\circ$ . . . . .	11
Figure 10. Instantaneous computed pressures, jet on, $M = 0.11$ , $\alpha = 0^\circ$ . . . . .	11
Figure 11. Computed lift force, $M = 0.11$ , $\alpha = 0^\circ$ . . . . .	12
Figure 12. Computed drag force, $M = 0.11$ , $\alpha = 0^\circ$ . . . . .	12
Figure 13. Computed lift force for various angles of attack, $M = 0.11$ . . . . .	13
Figure 14. Computed drag force for various angles of attack, $M = 0.11$ . . . . .	14
Figure 15. Computed lift force for various angles of attack, $M = 0.11$ , for a longer time period . . . . .	14
Figure 16. Computed change in lift force attributable to jet at various angles of attack, $M = 0.11$ , $\alpha = 0^\circ$ . . . . .	15

INTENTIONALLY LEFT BLANK

---

## **Acknowledgments**

---

This work was accomplished as part of a research project on micro-adaptive flow control sponsored and jointly funded by the Defense Advanced Research Projects Agency and the U.S. Army Research Laboratory (ARL). The author wishes to thank the members of the project team consisting of Georgia Tech Research Institute and Metacomp Technologies for their technical assistance. The scientific visualization work of R. Angelini of ARL and the computational support of the ARL Major Shared Resource Center are greatly appreciated.

INTENTIONALLY LEFT BLANK

---

## 1. Introduction

---

The prediction of aerodynamic coefficients for projectile configurations is essential in the assessment of the performance of new designs. Accurate determination of aerodynamics is critical to the low-cost development of new advanced guided projectiles, rockets, missiles, and smart munitions. Fins, canards, and jets can be used to provide control for maneuvering projectiles and missiles. The flow fields associated with these control mechanisms for the Army weapons are complex, involving three-dimensional (3-D) shock-boundary layer interactions, jet interaction with the free stream flow, and highly viscous dominated separated flow regions [1, 2, 3]. The jet interference can extend over significant portions of the projectile and must be modeled correctly. For missiles, jet thrusters have been studied over a number of years to provide high-speed aerodynamic control. These thrusters interact with the surrounding flow field, and the resulting jet interaction flow field again is complex. Recently, several studies have shown that tiny micro-electro-mechanical system or synthetic unsteady jets can significantly alter the flow field and pressure distributions for airfoils and cylinders [4, 5, 6]. These synthetic jets are active control devices with zero net mass flux and are intended to produce the desired control of the flow field through momentum effects. Many parameters such as jet location, jet velocity, and actuator frequency can affect the flow control phenomenon.

Smith and Glezer [4] have conducted an excellent study of the flow control by synthetic jets to provide increased fundamental understanding of the flow physics. Amitay et al. [5] experimentally investigated flow separation control on a cylinder using synthetic jet actuators. Their work showed that the interaction of the synthetic jet with the free stream flow resulted in a virtual modification of the body shape and significantly increased the lift force as a result of the flow reattachment. Aerodynamic flow control over an unconventional airfoil has also been demonstrated by Amitay et al. [6] to enhance post-stall performance with actuators operating at frequencies higher than the characteristic frequency of the airfoil. The synthetic jets are also being investigated for possible applications to improve heat transfer and drag reduction and to enhance mixing [7] in combustors, etc. The present analysis involves these synthetic jets for projectile aerodynamic control. The emphasis in the present research is to provide insight into the interaction of these unsteady jets with the free stream flow and to determine the feasibility of these jets for aerodynamic control of a subsonic projectile.

Computational and experimental data for these jet interactions are very limited. Simple theories cannot predict the complex flow fields associated with the jet interaction, and experimental tests are very expensive. To help reduce experimental costs, computational fluid dynamics (CFD) are being used to predict these complex flows and to provide detailed pressure and force and moment data. There have been several recent numerical studies [8, 9] of flow separation control with synthetic jet actuators. He and Kral [8] have used Reynolds-averaged Navier-Stokes

(RANS) to study the effect of jet location and jet-forcing frequency on the lift and drag forces on an airfoil. The jet actuator was shown to increase the time-averaged lift but also increased the amplitude of oscillation. Lee and Goldstein [9] have used the direct numerical simulation (DNS) to model a two-dimensional (2-D) synthetic jet. Although this simulation produced very good results, the use of DNS in practical 3-D flows of interest is prohibitive because of its computing resources requirement. Even large eddy simulations (LES) [10], in which large eddies are computed directly and the small scales are modeled, require a large computational cost compared to RANS simulations. While the RANS method works well for steady flows, the accuracy of this method for unsteady flows may be less than desired. Since the large energy-containing eddies are computed by the LES method, this technique is more capable of handling unsteady shear layers and wakes, etc. Recently, therefore, a hybrid approach [11, 12] that combines RANS and LES has been developed to solve practical problems of interest involving unsteady flows at a reasonable computational cost. Both RANS and hybrid RANS-LES models have been used in the present study.

The advanced CFD capability used here solves the Navier-Stokes equations [13 through 16] and incorporates unsteady boundary conditions for the simulation of the synthetic jets. Also, a hybrid RANS-LES turbulence model [12] was used for the accurate numerical prediction of unsteady jet flows. Numerical flow field computations have been made for steady and unsteady jets for a projectile configuration at a low subsonic speed.

The following sections describe the numerical procedure and the computed results obtained. Results obtained for a projectile configuration are presented at Mach 0.11 and several angles of attack,  $0^\circ$  to  $4^\circ$ . Computed data have been compared with experimental data provided by the Georgia Tech Research Institute (GTRI) [17]<sup>1</sup>.

---

## 2. Solution Technique

---

The complete set of 3-D time-dependent Navier-Stokes equations is solved in a time-accurate manner for simulations of unsteady jets. A commercially available code, CFD++ [14, 15, 16], is used for the time-accurate unsteady CFD simulations. The basic numerical framework in the code contains unified grid, unified physics, and unified computing features. The user is referred to these references for details of the basic numerical framework. Here, only a brief synopsis of this framework and methodology is given.

The 3-D, time-dependent RANS equations are solved by the following finite volume method:

---

<sup>1</sup>Private communication with J. McMichael, Georgia Tech Research Institute.

$$-\frac{d}{dt} \int_V \mathbf{W} dV + \oint_V [\mathbf{F} - \mathbf{G}] dA = \int_V \mathbf{H} dV \quad (1)$$

in which  $\mathbf{W}$  is the vector of conservative variables,  $\mathbf{F}$  and  $\mathbf{G}$  are the inviscid and viscous flux vectors, respectively,  $\mathbf{H}$  is the vector of source terms,  $V$  is the cell volume, and  $A$  is the surface area of the cell face.

The numerical framework of CFD++ is based on the following general elements:

1. unsteady compressible and incompressible Navier-Stokes equations with turbulence modeling (unified physics);
2. unification of Cartesian, structured curvilinear, and unstructured grids, including hybrids (unified grid);
3. unification of treatment of various cell shapes including 3-D hexahedral, tetrahedral, and triangular prism cells, 2-D quadrilateral and triangular cells, and one-dimensional linear elements (unified grid);
4. treatment of multi-block patched aligned (nodally connected), patched nonaligned, and overset grids (unified grid);
5. total variation diminishing discretization based on a new multi-dimensional interpolation framework;
6. Riemann solvers providing proper signal propagation physics, including versions for preconditioned forms of the governing equations;
7. consistent and accurate discretization of viscous terms via the same multidimensional polynomial framework;
8. point-wise turbulence models not requiring knowledge of distance to walls;
9. versatile boundary condition implementation, including a rich variety of integrated boundary condition types for the various sets of equations; and
10. implementation on massively parallel computers based on the distributed memory message-passing model via native message-passing libraries or message-passing interface, parallel virtual machine, etc. (unified computing).

The code has brought together several ideas about convergence acceleration to yield a fast methodology for all flow regimes. The approach can be labeled as a “preconditioned implicit relaxation” scheme. It combines three basic ideas: (1) implicit local time stepping, (2) relaxation, and (3) preconditioning. Preconditioning the equations ideally equalizes the eigenvalues of the inviscid flux Jacobians and removes the stiffness arising from large discrepancies between the flow and sound velocities at low speeds. The use of an implicit scheme circumvents the stringent stability limits suffered by their explicit counterparts, and

successive relaxation allows cells to be revised as information becomes available and thus aids convergence. These features of the code have been extremely useful in the present numerical simulations at very low subsonic speeds.

The CFD++ code also uses a multi-dimensional interpolation that more accurately represents local behavior of flow-dependent variables. Second order discretization was used for the flow variables and the turbulent viscosity equation. The turbulence closure is based on topology-parameter-free formulations. Two-equation and higher order hybrid RANS-LES turbulence models were used for the computation of turbulent flows. These models are ideally suited to unstructured bookkeeping and massively parallel processing because of their independence from constraints related to the placement of boundaries and/or zonal interfaces.

For computations of unsteady jet interaction flow fields that are of interest here, dual time stepping as described in Section 2.1 was used to for time accuracy. In addition, special jet boundary conditions were developed and used for numerical modeling of synthetic jets.

## **2.1 Dual Time Stepping**

CFD++ is often used in the “dual time-stepping mode” to perform transient flow simulations. The term “dual time step” implies the use of two time steps. The first is an “outer” or global (and physical) time step that corresponds to the time discretization of the physical time variation term. This time step can be chosen directly by the user and is typically set to a value to represent 1/100 of the period of oscillation expected or forced in the transient flow. This time step is applied to every cell (not separately varying).

An artificial or “inner” or “local” time variation term is added to the basic physical equations. This time step and corresponding “inner iteration” strategy is chosen to help satisfy the physical transient equations to the desired degree. If the inner iterations converge, then the outer physical transient equations (their discretization) are satisfied exactly otherwise, approximately. For the inner iterations, the time step is allowed to vary spatially. Also, relaxation with multi-grid (algebraic) acceleration is employed to reduce the residues of the physical transient equations. It is found that an order of magnitude reduction in the residues is usually sufficient to produce a good transient iteration. This may require a few internal iterations to achieve (between 3 and 10, depending on the magnitude of the outer time step), the nature of the problem, the nature of the boundary conditions, and the consistency of the mesh with respect to the physics at hand.

## **2.2 Unsteady Jet Boundary Condition**

CFD++ has a large collection of boundary conditions (BC). Each BC is encoded as a basic form, along with a collection of modifiers. One particular BC used for the simulations presented here is a “oscillating jet” BC. In its basic form, it is a steady inflow/outflow BC wherein the user supplies the velocity normal to the boundary along with static temperature and any turbulence quantities. When the velocity provided is negative, it is considered to be an inflow and when it is positive, it is treated as an outflow. In the case of inflow, the static temperature and turbulence

quantities are used, along with the inflow velocity. In the case of outflow, only the velocity is used. At inflow, the tangential component of velocity is set to zero and at outflow, the tangential component is extrapolated from the interior. At outflow, all primitive variables except normal velocity are extrapolated from the interior. At inflow, the static pressure is taken from the interior.

The first modifier available for this BC allows the velocity to oscillate. The base velocity is multiplied by an amplitude that varies as  $\sin(2\pi ft)$  in which  $f$  is the frequency of the oscillation. Thus, the oscillating velocity can cycle from being positive to being negative and back within each period (or from being negative to positive and back, based on the sign of the input for the basic BC formulation).

A second modifier permits the steady or oscillating inflow/outflow to be on over-certain time intervals and off during other intervals. During “on” periods, the basic or the basic multiplied by the oscillating amplitude multiplier (first modifier) is used. During “off” periods, the amplitude is set to zero. Therefore, when the jet velocity is zero, the boundary condition behaves like a no-slip condition.

### 2.3 Hybrid RANS-LES Model

Currently, the two most popular forms of turbulence closure, namely, ensemble-averaged models (typically based on the RANS equations) and LES with a sub-grid-scale model, face a number of unresolved difficulties. Specifically, existing LES models have met with problems related to the accurate resolution of the near-wall turbulent stresses. In the near-wall region, the foundations of large eddy simulation are less secure, since the sizes of the (anisotropic) near-wall eddies approach those of the Kolmogorov scale, requiring a mesh resolution approaching that of a direct numerical simulation. On the other hand, existing ensemble-averaged turbulence models are limited by their empirical calibration. Their representation of small scale flow physics cannot be improved by refining the mesh, and over short time scales, they tend to be overly dissipative with respect to perturbations around the mean, often suppressing unsteady motion altogether.

While LES is an increasingly powerful tool for unsteady turbulent flow prediction, it is still prohibitively expensive. To bring LES closer to becoming a design tool, a hybrid RANS-LES approach based on limited numerical scales (LNS) has been recently developed by Metacomp Technologies [12]. This approach combines the best features of RANS and LES in a single modeling framework. The LNS model is formulated from an algebraic or differential Reynolds stress model, in which the sub-grid stresses are limited by the numerically computed local length scale and velocity scale products. LNS thus behaves like its parent RANS model on RANS-type grids but reverts to an *anisotropic* LES sub-grid model as the mesh is refined locally, thereby reaching the correct (DNS) fine grid limit. Locally embedded regions of LES may be achieved automatically through local grid refinement, while the superior near-wall stress predictions of the RANS model are preserved, removing the need of *ad hoc* topography-parameter-based wall damping.

The LNS hybrid formulation is well suited to the simulation of unsteady flows, including mixing flows, and contains no additional empirical constants beyond those appearing in the original RANS and LES sub-grid models. With this method, a regular RANS-type grid is used except in isolated flow regions where denser, LES-type mesh is used to resolve critical unsteady flow features. The hybrid model transitions smoothly between an LES calculation and a cubic k-model, depending on grid fineness. A somewhat finer grid was placed around the body and near the jet, and the rest of the flow field is occupied by a coarser, RANS-like mesh.

To date, the LNS technique has been used successfully on a number of unsteady flows. Examples include flows over cavities, flows around blunt bodies, flows around airfoils and wings at high angle of attack, separation suppression via synthetic jets, forced and natural convection flows in a room, and mixing flows in nozzles.

---

### 3. Results

---

Time-accurate unsteady numerical computations that use viscous Navier-Stokes methods were performed to predict the flow field and aerodynamic coefficients on the subsonic projectile for “jet-on” conditions. Three-dimensional numerical computations have been performed for the projectile configuration with jet interaction using CFD++ code at a subsonic Mach number of 0.11 and several angles of attack from 0° to 4°. The preconditioned version of the CFD++ code was used to obtain efficient numerical solution at low speed. A point-wise two-equation turbulence model was used and integrated all the way to the wall. For modeling of the unsteady synthetic jets, a hybrid RANS-LES approach [12] was used. For computations of these unsteady jets, full 3-D computations are performed and no symmetry was used. Computed results are compared with the available experimental wind tunnel data provided GTRI<sup>2</sup>.

For computational validation purposes, CFD was first used to compute the flow for an isolated 2-D jet case shown in Figure 1. This figure shows a schematic diagram of a 2-D synthetic jet along with a flow picture obtained from the experiment [4]. Such synthetic jets are active control devices with zero net mass flux and are intended to produce the desired control of the flow field through momentum effects. Here, the jet width is 0.5 mm and the peak jet velocity is 20 m/s. The jet actuator operates at a frequency of 1000 Hz. In the numerical computations, unsteady jet boundary conditions were applied at the jet exit and the actual cavity was not modeled. A sinusoidal variation was used for the jet exit velocity with a peak amplitude of 20 m/s. Computed velocity and vorticity contours are shown in Figure 2. The time-averaged jet centerline velocity over many cycles is compared with available experimental data in Figure 3 and is found to be in reasonable agreement. As shown in the experiment and the computations,

---

<sup>2</sup>Private communication with J. McMichael, Georgia Tech Research Institute.

the time-averaged centerline velocity is decreased with increasing distance away from the jet exit (increasing  $z$  in the  $x$ -axis in Figure 3). The CFD technique described earlier was then applied to compute the flow over a projectile at subsonic speeds.

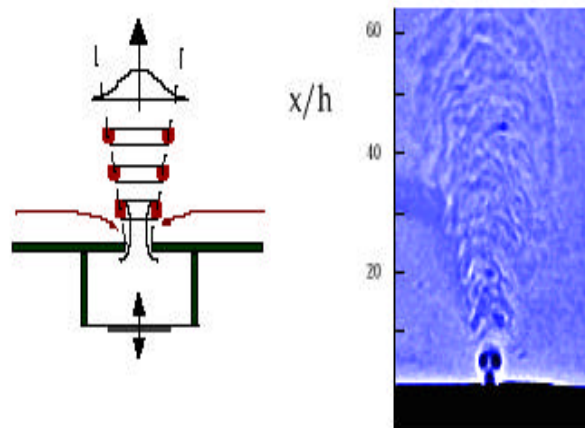


Figure 1. Schematic of a 2-D unsteady jet in the experiment.

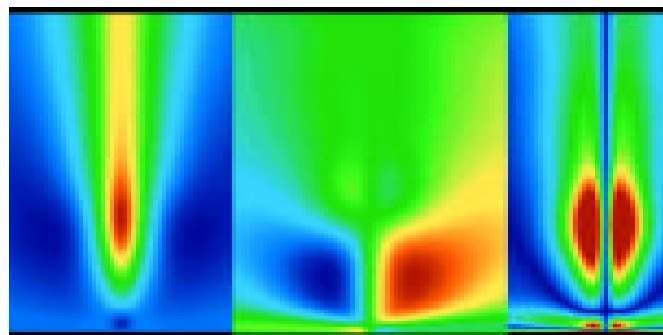


Figure 2. Contours of velocity components ( $u, v$ ) and vorticity (from left to right).

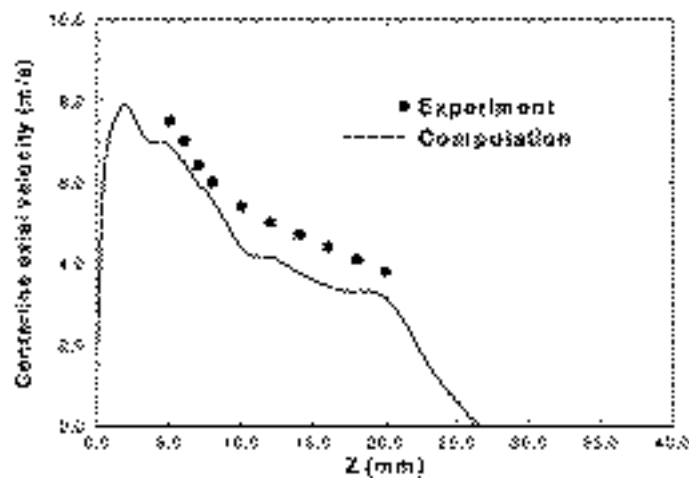


Figure 3. Variation of time-averaged centerline jet velocity with distance from the wall.

The subsonic projectile is a 1.8-caliber ogive-cylinder configuration (see Figure 4). Here, the primary interest is in the development and application of CFD techniques for accurate simulation of projectile flow field in the presence of unsteady jets. The first step here was to obtain the steady state results for the same projectile without the jet. The converged “jet-off” steady state solution was then used as the starting condition for the computation of the time-accurate unsteady flow field for the projectile with synthetic jets. Computations were also performed for the steady jet cases. The jet locations on the projectile are shown in Figure 5. The jet conditions were specified at the exit of the jet for steady (fixed jet velocity) and unsteady (sinusoidal variation in jet velocity) jets. The jet conditions specified include the jet pressure, density, and velocity components. The flow field inside the tiny jet cavity is not computed. For the unsteady jet case, time-dependent jet boundary conditions are applied at the jet exit. Numerical computations have been made for these jet cases at a Mach number,  $M = 0.11$ , and at an angle of attack,  $\alpha = 0^\circ$ . The jet width was 0.32 mm, the jet slot half-angle was  $18^\circ$ , and the peak jet velocity used was 31 m/s operating at a frequency of 1000 Hz.



Figure 4. Projectile model geometry.



Figure 5. Aft-end geometry showing the jet location.

A computational grid expanded near the vicinity of the projectile is shown in Figure 6. Grid points are clustered near the jet as well as the boundary layer regions to capture the flow regions' high gradients. The computational grid has 211 points in the streamwise direction, 241 in the circumferential direction, and 80 in the normal direction. The unsteady simulation took thousands of hours of central processing unit time on a Silicon Graphics Origin computer running with 24 processors.

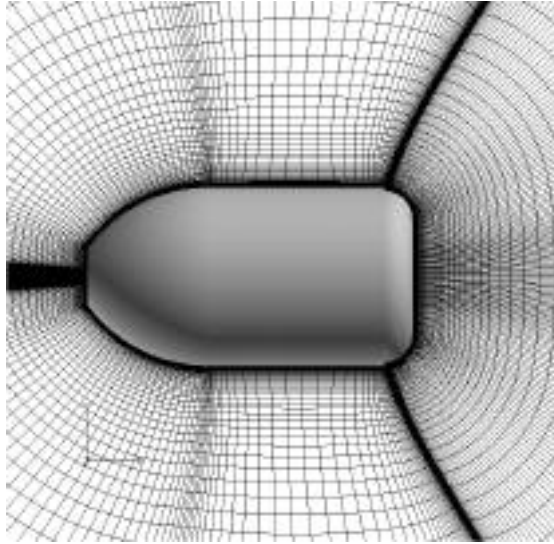


Figure 6. Computational grid near the projectile.

Computed pressure contours for the jet-off case at  $M = 0.11$  and  $\alpha = 0^\circ$  are shown in Figure 7. This figure shows a high pressure region near the nose and low pressures in the near wake. Computed velocity vectors for this case are shown in Figure 8. The re-circulatory flow regions in the wake and near the step upstream from the base are clearly evident. As seen in this figure, the flow field in the base region is fairly symmetrical. The flow field results for the synthetic jet-on case are shown in Figures 9 and 10. These figures show the qualitative flow features near the jet as well as the base region of the projectile. Figure 9 shows the velocity vectors at a given instant in time. It clearly shows the flow in the base region to be asymmetric because of the interaction of the unsteady jet. The shear layer from the free stream flow resulting from the step corner upstream from the base interacts with the unsteady jet and deteriorates just a short distance downstream from the jet. The jet has a strong effect on the pressure distribution upstream and downstream from the jet location (see Figure 10). The pressure field upstream and downstream from the jet is clearly affected by the jet flow, depending on whether the flow is entering or leaving the cavity. The computed flow field again is asymmetrical. Figure 10 also shows regions of alternating low and high pressure just downstream from the jet, indicating vorticity being shed from the jet exit into the base region flow.

The resulting surface pressures from the unsteady flow fields are integrated to obtain the aerodynamic forces and moments. The computed axial force and normal force are shown in Figures 11 and 12 as a function of time, respectively. These computed results clearly indicate the unsteady nature of the flow field. These forces are found to change as a function of time. Changes in the drag force are smaller than those of the lift force over the first 50 ms. In both figures, computed results obtained with unsteady RANS (URANS) as well as the hybrid RANS-LES approach referred to here as the LNS, are compared to each other. As shown in Figure 11, LNS and URANS both produce a non-zero lift force attributable to the jet at 0 degree angle of attack. The lift computed by the URANS approach is about half that computed by the LNS

approach. As shown in Figure 12, the drag force variation as a function of time is small with the LNS method, whereas the variation is almost negligible with URANS. Although not shown here, the pitching moment also shows a variation similar to that of the lift force.

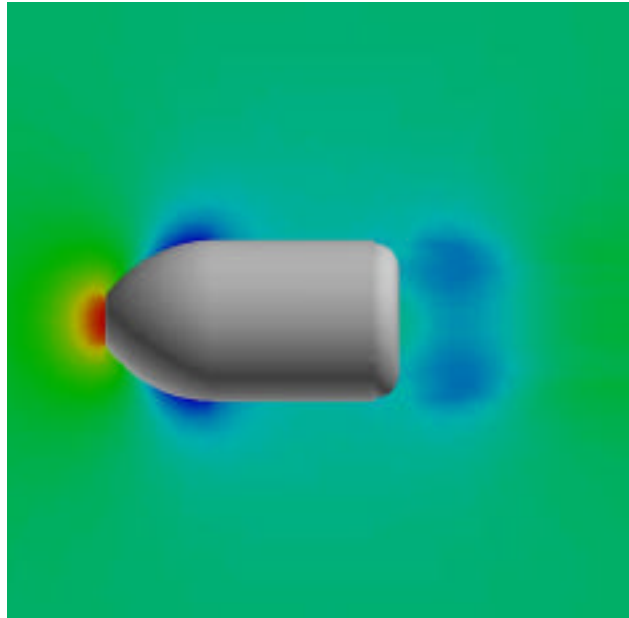


Figure 7. Computed pressures, jet off,  $M = 0.11$ ,  $\alpha = 0^\circ$ .

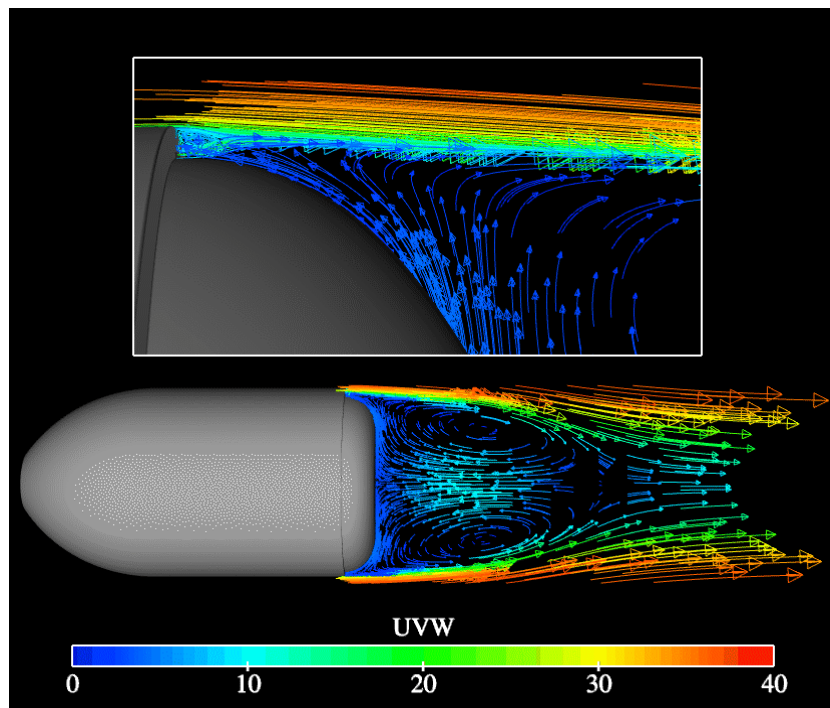


Figure 8. Computed velocity vectors, jet off,  $M = 0.11$ ,  $\alpha = 0^\circ$ .

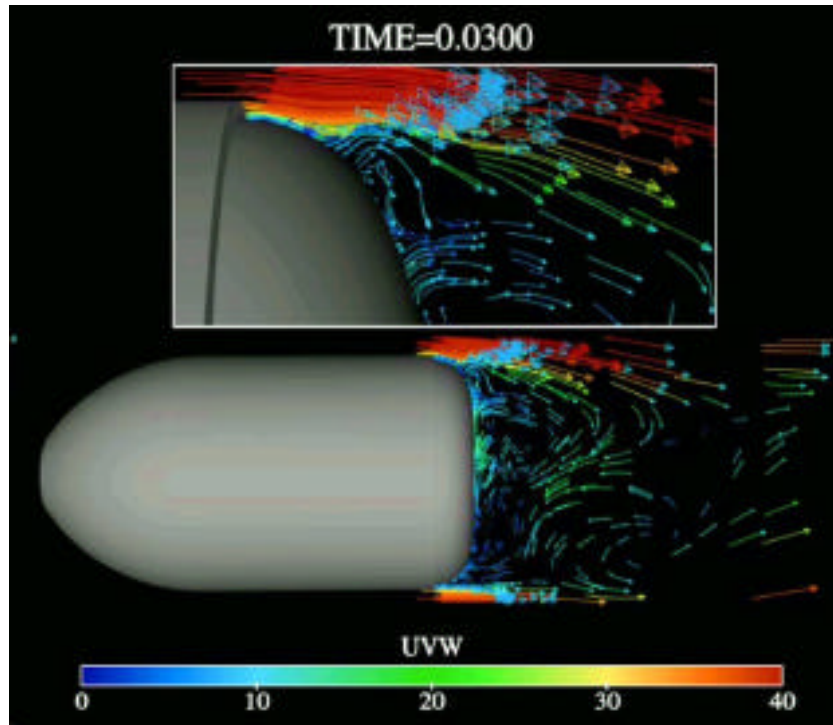


Figure 9. Instantaneous computed velocity vectors, jet on,  $M = 0.11$ ,  $\alpha = 0^\circ$ .

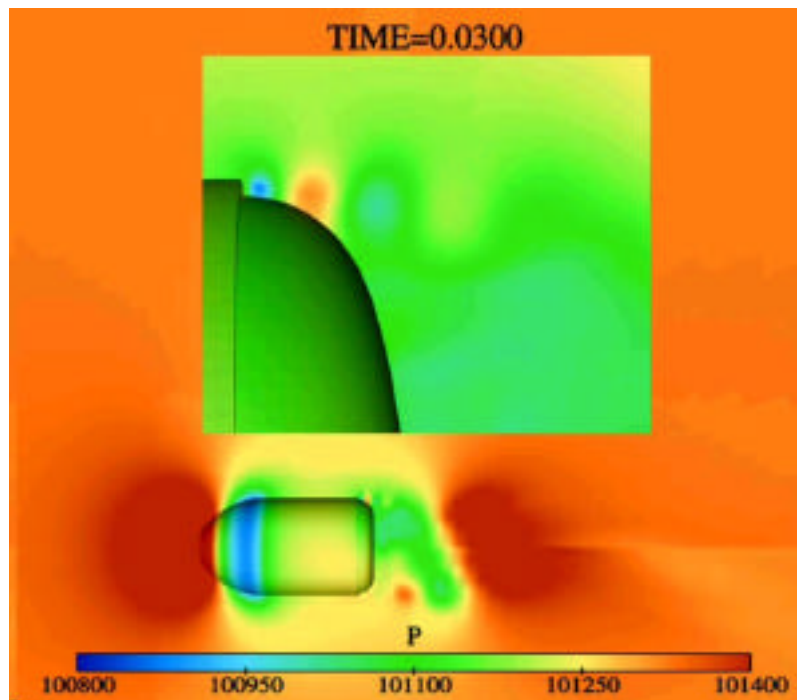


Figure 10. Instantaneous computed pressures, jet on,  $M = 0.11$ ,  $\alpha = 0^\circ$ .

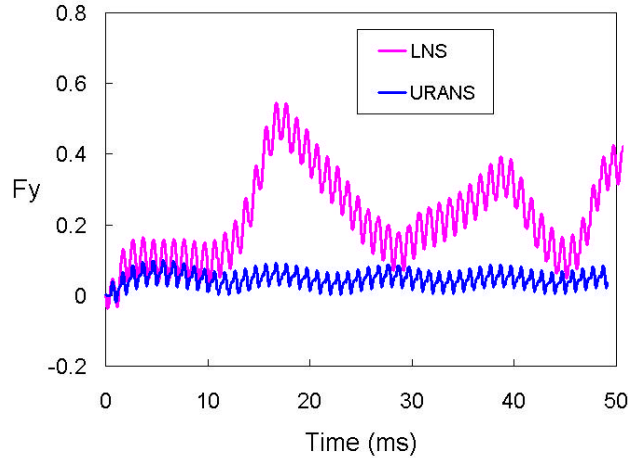


Figure 11. Computed lift force,  $M = 0.11$ ,  $\alpha = 0^\circ$ .

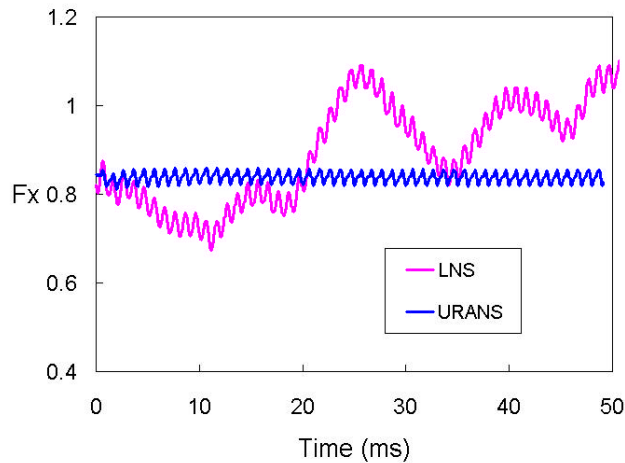


Figure 12. Computed drag force,  $M = 0.11$ ,  $\alpha = 0^\circ$ .

Figures 13 and 14 show the time histories of the lift and drag forces, respectively, for various angles of attack. These computed results are obtained with the LNS turbulence model. Figure 13 shows the increase in the lift force resulting from the jet interaction for all angles of attack considered. The values for the jet-off condition correspond to time zero. As shown in Figure 14, the drag force is also seen to increase somewhat because of the jet interaction, but the effect of angle of attack on the drag force is rather small.

The unsteady interaction of the synthetic jet and the wake flow of the projectile usually require hundreds of cycles of the jet operations before a truly unsteady periodic flow is established. Computations were extended to 50 additional cycles of jet operation for 0- and 4-degree angles of attack. These computed results are shown in Figure 15 as a function of time until 100 ms. Also, in order to test the time accuracy, the time step was reduced from 0.025 ms to 0.00833 ms approximately at time 70 ms. Although not shown here, the number of inner time steps in the dual time-stepping scheme used here was also varied and the results were found to remain

essentially unaltered. As can be seen, the mean value of the lift force for 0- and 4-degree angles of attack did not change much. For the 0-degree angle of attack case, the mean value of the lift force was calculated to be about 0.18 Newton, resulting from the unsteady jet interaction. Similarly, time-averaged mean values of the lift forces at other angles of attack ( $\alpha = 2$  and 4) were computed. The difference between these computed mean values of the lift force and the corresponding lift at jet-off condition then yields the net change in the lift force attributable to the jet interaction. Figure 16 shows the change in lift force attributable to the jet interaction at various angles of attack. The computed results here are found to be generally in good agreement with the experimentally [17]<sup>3</sup> obtained lift force attributable to the jet. As seen in both CFD and the experiment, the change in lift attributable to the jet interaction is almost constant with angle of attack from 0° to 4°.

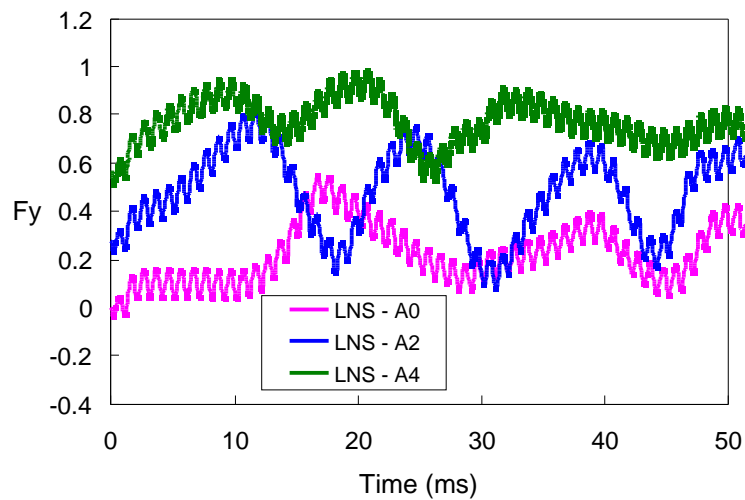


Figure 13. Computed lift force for various angles of attack,  $M = 0.11$ .

Also, a large number of CFD data sets were saved at regular intervals to analyze the fully unsteady periodic nature of the flow field which required huge computer resources in terms of storage and flow visualization. The computed results obtained thus far have been used to determine the feasibility of the synthetic jets to provide control authority. The next challenge is to use the current methods with the same projectile but with spin. Future efforts will require large unsteady numerical computations to optimize the number and locations of the synthetic jets. It is anticipated that multiple jets may be required to provide the control authority needed for maneuvering a subsonic projectile and will require the use of a coupled CFD and controls technique to divert control authority by means of a jet.

<sup>3</sup>Private communication with J. McMichael, Georgia Tech Research Institute.

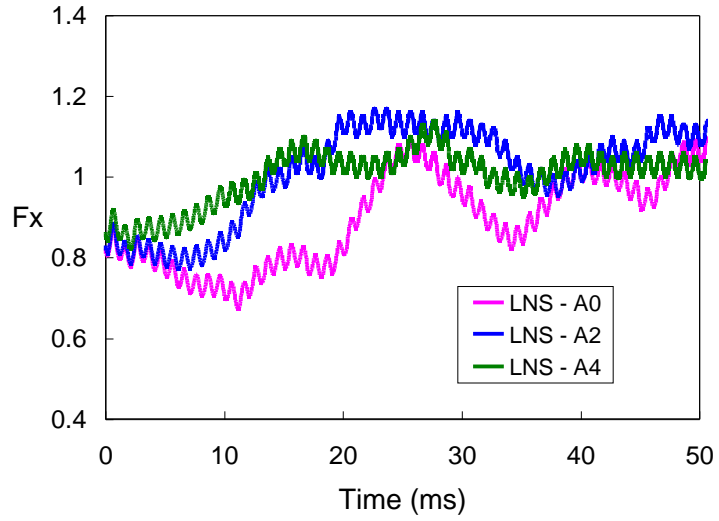


Figure 14. Computed drag force for various angles of attack,  $M = 0.11$ .

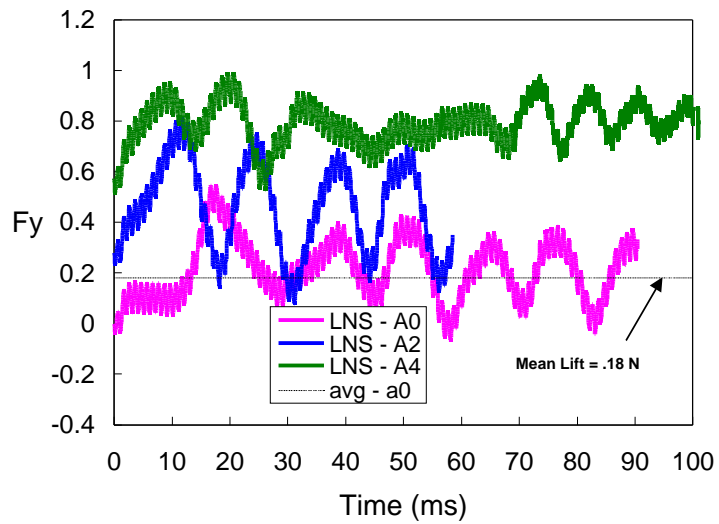


Figure 15. Computed lift force for various angles of attack,  $M = 0.11$ , for a longer time period.

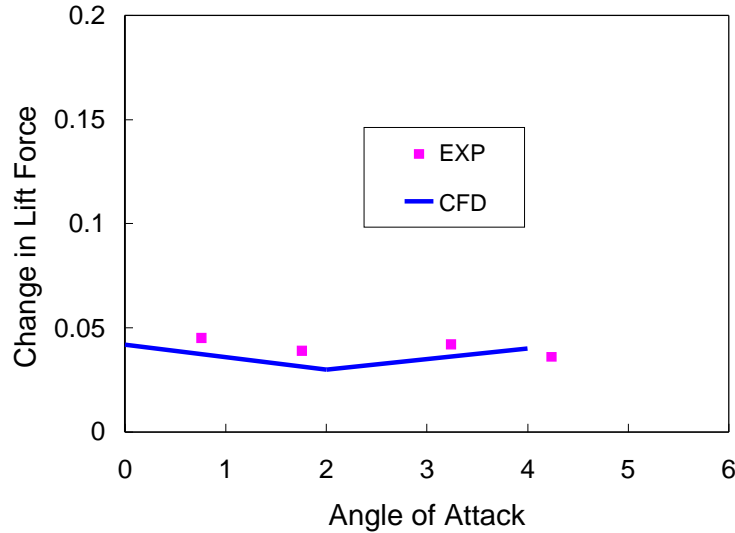


Figure 16. Computed change in lift force attributable to jet at various angles of attack,  $M = 0.11$ ,  $\alpha = 0^\circ$ .

---

#### 4. Concluding Remarks

---

This report described a computational study undertaken to determine the aerodynamic effect of tiny synthetic jets as a means to provide the control authority needed to maneuver a projectile at low subsonic speeds. Computed results have been obtained at a low subsonic speed and 0 degree angle of attack for a subsonic projectile via the Navier-Stokes computational technique and advanced turbulence models. Qualitative flow field features show the interaction of synthetic jet with the free stream flow and the large extent of influence upstream and downstream from the jet. Unsteady jet results obtained for a 2-D jet are compared with the data and are found to be in reasonable agreement. The unsteady jet in the case of the subsonic projectile is shown to substantially alter the flow field near the jet and the base region, which in turn affects the forces and moments even at 0 degree angle of attack. RANS and hybrid RANS-LES turbulence models were used in the computations at 0 degree angle of attack. The lift predicted by the RANS simulation is less than half the predicted lift with the hybrid model. The predicted changes in lift force attributable to the jet match well with the experimental data for various angles of attack from  $0^\circ$  to  $4^\circ$ .

The results show the potential of CFD to provide insight into the jet interaction flow fields and provide guidance as to the locations and sizes of the jets to generate the maximum control authority for maneuvering smart munitions. Current and future efforts are directed toward the addition of spin and yaw to these large unsteady synthetic jet computations for application to a spinning projectile. Future efforts will also include the optimization of the number and location of the synthetic jets as well as coupling of CFD and controls to accurately determine the control authority needed for maneuvering a subsonic spinning projectile.

---

## 5. References

---

1. Sahu, J., Heavey, K.R., Ferry, E.N. Computational Fluid Dynamics for Multiple Projectile Configurations. *Proceedings of the 3rd Overset Composite Grid and Solution Technology Symposium*, Los Alamos, NM, October 1996.
2. Sahu, J., Heavey, K.R., Nietubicz, C.J. Time-Dependent Navier-Stokes Computations for Submunitions in Relative Motion. *Sixth International Symposium on Computational Fluid Dynamics*, Lake Tahoe, NV, September 1995.
3. Meakin, R.L., Computations of the Unsteady Flow About a Generic Wing/Pylon/Finned-Store Configuration. *American Institute of Aeronautics and Astronautics (AIAA)*, **August 1992**, 92-4568-CP.
4. Smith B.L., Glezer, A. The Formation and Evolution of Synthetic Jets. *Journal of Physics of Fluids*, **September 1998**, 10(9), 2281-2297.
5. Amitay, M., Kibens, V., Parekh, D., Glezer, A., The Dynamics of Flow Reattachment over a Thick Airfoil Controlled by Synthetic Jet Actuators. *AIAA*, **January 1999**, Paper No. 99-1001.
6. Amitay, M., Smith, D.R., Kibens, V., Parekh, D., and Glezer, A. Aerodynamic Flow Control over an Unconventional Airfoil Using Synthetic Jet Actuators. *AIAA Journal*, **2001**, 39, 361-370.
7. Davis, S.A., Glezer, A., The Manipulation of Large and Small Scales in Coaxial Jets Using Synthetic Jet Actuators. *AIAA* **January 2000**, Paper No. 2000-0403.
8. He, Y., Kral, L., Post-Stall Control on an Airfoil using Localized Jet Actuators. *AIAA* **January 2000**, Paper No. 2000-0408.
9. Lee, C.Y., Goldstein, D.B. Two-Dimensional Synthetic Jet Simulation, *AIAA* **January 2000**, Paper No. 2000-0406.
10. Avancha, R., Pletcher, R.H. Large Eddy Simulation of the Turbulent Flow Past a Backward Facing Step, *AIAA* **January 2000**, paper No. 2000-0542.
11. Arunajatesan, S., Sinha, N., Towards Hybrid LES-RANS Computations of Cavity Flowfields, *AIAA* **January 2000**, Paper No. 2000-0401.
12. Batten, P., Goldberg, U.C., Chakravarthy, S. Sub-grid Turbulence Modeling for Unsteady Flow with Acoustic Resonance, *38th AIAA Aerospace Sciences Meeting*, **January 2000**, Paper 00-0473, Reno, NV.
13. Pulliam, T.H., Steger, J.L. On Implicit Finite-Difference Simulations of Three-Dimensional Flow. *AIAA Journal*, **February 1982**, 18(2), 159-167.

14. Peroomian, O., Chakravarthy, S., Goldberg, U.C. A “Grid-Transparent” Methodology for CFD. *AIAA* **1997**, Paper 97-07245.
15. Peroomian, O., Chakravarthy, S., Palaniswamy, S., Goldberg, U.C. Convergence Acceleration for Unified-Grid Formulation Using Preconditioned Implicit Relaxation. *AIAA* **1998**, Paper 98-0116.
16. Goldberg, U.C., Peroomian, O., Chakravarthy, S. A Wall-Distance-Free K-E Model With Enhanced Near-Wall Treatment. *ASME Journal of Fluids Engineering* **1998**, 120, 457-462.
17. Rinehart, C., McMichael, J.M., Glezer, A. Synthetic Jet-Based Lift Generation and Circulation Control on Axisymmetric Bodies. *AIAA Paper No. 2002-3168*.

NO OF  
COPIES ORGANIZATION

- 1 ADMINISTRATOR  
DEFENSE TECHNICAL INFO CTR  
ATTN DTIC OCA  
8725 JOHN J KINGMAN RD STE 0944  
FT BELVOIR VA 22060-6218
- 1 DIRECTOR  
US ARMY RSCH LABORATORY  
ATTN AMSRL CI AI R REC MGMT  
2800 POWDER MILL RD  
ADELPHI MD 20783-1197
- 1 DIRECTOR  
US ARMY RSCH LABORATORY  
ATTN AMSRL CI LL TECH LIB  
2800 POWDER MILL RD  
ADELPHI MD 20783-1197
- 1 DIRECTOR  
US ARMY RSCH LABORATORY  
ATTN AMSRL D D SMITH  
2800 POWDER MILL RD  
ADELPHI MD 20783-1197
- 2 USAF WRIGHT AERONAUTICAL  
LABORATORIES  
ATTNAFWAL FIMG  
DR J SHANG  
MR N E SCAGGS  
WPAFB OH 45433-6553
- 1 COMMANDER  
NAVAL SURFACE WARFARE CNTR  
ATTN CODE B40 DR W YANTA  
DAHLGREN VA 22448-5100
- 1 COMMANDER  
NAVAL SURFACE WARFARE CNTR  
ATTN CODE 420 DR A WARDLAW  
INDIAN HEAD MD 20640-5035
- 4 DIR NASA LANGLEY RSCH CTR  
ATTN TECH LIBRARY J SOUTH  
D M BUSHNELL M J HEMSCH  
LANGLEY STATION  
HAMPTON VA 23665
- 4 DIR NASA AMES RSCH CTR  
ATTN T 27B-1 L SCHIFF MS 258 M RAI  
T 27B-1 T HOLST MS 258 1 B MEAKIN  
MS 237-2 D CHAUSSEE  
MS T27B-2 M AFTOSMIS  
MS T27B-2 J MELTON  
MOFFETT FIELD CA 94035

NO OF  
COPIES ORGANIZATION

- 3 AIR FORCE ARMAMENT LAB  
ATTN AFATL/FXA S C KORN  
B SIMPSON D BELK  
EGLIN AFB FL 32542-5434
- 2 AFRL/MNAV  
ATTN G ABATE J ANTTONEN  
101 W EGLIN BLVD STE 219  
EGLIN AIR FORCE BASE FL 32542
- 4 CDR US ARMY TACOM ARDEC  
ATTN AMSTA AR FSF T W KOENIG  
H HUDGINS J GRAU C NG  
BLDG 382  
PICATINNY ARSENAL NJ 07806-5000
- 1 CDR US ARMY TACOM ARDEC  
ATTN AMCPM DS MO P J BURKE  
BLDG 162S  
PICATINNY ARSENAL NJ 07806-5000
- 1 CDR US ARMY TACOM  
ATTN AMSTA AR CCH B P VALENTI  
BLDG 65-S  
PICATINNY ARSENAL NJ 07806-5001
- 1 CDR US ARMY ARDEC  
ATTN SFAE FAS SD M DEVINE  
PICATINNY ARSENAL NJ 07806-5001
- 1 AEROPREDICTION INC  
ATTN F MOORE  
9449 GROVER DRIVE STE 201  
KING GEORGE VA 22485
- 2 UNIV OF CALIFORNIA DAVIS  
DEPT OF MECHANICAL ENG  
ATTN PROF H A DWYER PROF M HAFEZ  
DAVIS CA 95616
- 1 AEROJET ELECTRONICS PLANT  
ATTN D W PILLASCH  
B170 DEPT 5311  
P O BOX 296  
1100 WEST HOLLYVALE ST  
AZUSA CA 91702
- 1 MASS INST OF TECHNOLOGY  
ATTN TECH LIBRARY  
77 MASSACHUSETTS AVE  
CAMBRIDGE MA 02139
- 1 LOS ALAMOS NATL LAB  
ATTN MS G770 WM HOGAN  
LOS ALAMOS NM 87545

NO OF  
COPIES ORGANIZATION

- 1 NAVAL AIR WARFARE CTR  
ATTN MS 3 D FINDLAY  
BLDG 2187  
PATUXENT RIVER MD 20670
- 3 DIR SANDIA NATL LABS  
ATTN DIV 1554 DR W OBERKAMPF  
DIV 1554 DR F BLOTTNER  
DIV 1636 DR W WOLFE  
ALBUQUERQUE NM 87185
- 1 METACOMP TECHNOLOGIES INC  
ATTN S R CHAKRAVARTHY  
650 HAMPSHIRE RD STE 200  
WESTLAKE VILLAGE CA 91361-2510
- 1 ADVANCED TECHNOLOGY CTR  
ARVIN/CALSPAN  
AERODYNAMICS RSCH DEPT  
ATTN DR M S HOLDEN  
PO BOX 400  
BUFFALO NY 14225
- 1 UNIV OF IL AT URBANA CHAMPAIGN  
DEPT OF MECH AND INDUS ENG  
ATTN DR J C DUTTON  
URBANA IL 61801
- 1 UNIV OF MARYLAND  
DEPT OF AEROSPACE ENG  
ATTN DR J D ANDERSON JR  
COLLEGE PARK MD 20742
- 1 UNIV OF TEXAS  
DEPT OF AEROSPACE ENG MECHANICS  
ATTN DR D S DOLLING  
AUSTIN TX 78712-1055
- 1 CDR USAAMCOM  
ATTN AMSAM RD SS G LANDINGHAM  
REDSTONE ARSENAL AL 35898-5252
- 2 ARROW TECH ASSOC  
ATTN W HATHAWAY R WHYTE  
1233 SHELBURNE RD STE D8  
SOUTH BURLINGTON VT 05403

ABERDEEN PROVING GROUND

- 2 DIRECTOR  
US ARMY RSCH LABORATORY  
ATTN AMSRL CI LP (TECH LIB)  
BLDG 305 APG AA

NO OF  
COPIES ORGANIZATION

- 2 DIRECTOR  
US ARMY RSCH LABORATORY  
ATTN AMSRL WM JILL SMITH  
T ROSENBERGER  
BLDG 4600
- 1 DIRECTOR  
US ARMY RSCH LABORATORY  
ATTN AMSRL WM B A W HORST JR  
BLDG 4600
- 1 DIRECTOR  
US ARMY RSCH LABORATORY  
ATTN AMSRL WM BA D LYON  
BLDG 4600
- 2 DIRECTOR  
US ARMY RSCH LABORATORY  
ATTN AMSRL WM BC P PLOSTINS  
J SAHU  
BLDG 390
- 1 DIRECTOR  
US ARMY RSCH LABORATORY  
ATTN AMSRL CI N RADHAKRISHNAN  
BLDG 394
- 1 DIRECTOR  
US ARMY RSCH LABORATORY  
ATTN AMSRL CI H C NIETUBICZ  
BLDG 328
- 1 DIRECTOR  
US ARMY RSCH LABORATORY  
ATTN AMSRL CI HC R NOAK  
BLDG 394
- 3 CDR US ARMY ARDEC  
FIRING TABLES BRANCH  
ATTN R LIESKE R EITMILLER  
F MIRABELLE  
BLDG 120